Analysis of Very High Throughput (VHT) at MAC and PHY Layers under MIMO Channel in IEEE 802.11ac WLAN

Gul Zameen Khan*, Ruben Gonzalez*, Eun-Chan Park**, Xin-Wen Wu*
*School of Information and Communication Technology, Griffith University, Australia
**Dept. of Information and Communication Engineering, Dongguk University, South Korea
gz.khan@griffithuni.edu.au, r.gonzalez@griffith.edu.au, ecpark@dongguk.edu, x.wu@griffith.edu.au

***Abstract*—This paper analyses the very high system throughput of IEEE 802.11ac by taking into consideration the key features of MAC and PHY layers under a Multiple In Multiple Out (MIMO) channel. Throughput at the MAC layer is calculated from the transmission probability, contention window and transmission stage. Likewise, the new critical attributes of 802.11ac PHY (i.e. modulation and coding schemes, spatial streams, and channel bandwidth) are used to determine the throughput at the PHY layer. To this end, a theoretical model is formulated at the MAC and PHY layers followed by a system model of MIMO multipath fading channel for 802.11ac. The system model is verified by simulation analysis. The results compare theoretical and simulation findings for different sets of parameters. Furthermore, important trends and trade-offs are identified between system throughput and (MAC + PHY) features as a function of number of contending stations and payload size. The system throughput of 802.11ac networks is significantly improved due to the addition of new PHY features. However, the system may degrade upto 50% in terms of symbol reception in case of a high error-prone MIMO channel. The performance of 802.11ac systems is also analyzed under different MIMO TGn channel models in terms of Packet Error Rate (PER). Thus based on our simulation results, an appropriate channel model can be chosen for 802.11ac network under a given configuration to achieve a better performance.**

***Keywords*—Performance, analysis, throughput, MAC, physical, MIMO, multipath, fading, transmission probability, contention window, modulation, coding, spatial streams, channel bandwidth, channel model**

I. Introduction

Gigabit Wireless Local Area Networks (WLAN) is a state-of-the-art technology based on the emergence of new IEEE standard i.e., 802.11ac [1]. The standard achieves Very High Throughput (VHT) with the aid of efficient Modulation and Coding Schemes (MCS) such as 256-Quadrature Amplitude Modulation (QAM), explicit transmit beamforming, enhanced Multiple Input Multiple Output (MIMO) technology, and large bandwidth. Most of the leading vendors and manufacturers have already implemented 802.11ac in their Wi-Fi chipsets [2]. 802.11ac operates in 5 GHz band and can support a high data rate up to 6.933 Gb/s.

Currently, most of the literature available on 802.11ac focuses on improving the underlying technology of 802.11ac. This includes but is not limited to exploring Single User (SU) and Multi User (MU) MIMO, adding new Spatial Streams (SS), improving frame aggregation techniques, channel bonding, and incorporating advanced modulation and coding techniques in 802.11ac. In [3], a review of PHY layer features of 802.11ac is presented. The performance of MU-MIMO is analysed via a testbed. However, the chips used in the experiment are based on 802.11n [4]. In [5], the authors present a performance analysis of energy efficiency and interference in 802.11ac. It is shown that larger channels consume more power while the addition of more SS is energy efficient. However, the performance measurements are not verified by any theoretical model. Although a comparison of 802.11ac and 802.11n is drawn in [6] in terms of different frame aggregation techniques, other key features of 802.11ac have not been explored. Similarly, [7] discusses the requirement in MAC modifications and enhancements for downlink MU-MIMO transmission. In particular, it introduces the technique of enhancing Transmit Opportunity (TXOP) and the revised backoff procedures. In the same manner, the authors of [8] present a review of how the capacity can be estimated and optimized using Ekahau Site Survey tool in 802.11ac. Similarly, [9] presents a performance comparison between 802.11n and 802.11ac in terms of throughput for three MAC frame aggregation techniques under constant PHY conditions. For the most part, 802.11ac outperforms 802.11n due to its larger frames in error-free channel. On the contrary, the optimal frame size is determined by bit error in error-prone channel conditions. The paper however, considers only the frame size instead of other key factors of MAC and PHY layers. Similarly, an overview of static and dynamic channel selection methods is demonstrated in [10] with the help of simulations. It is shown that dynamic selection of a primary channel achieves high throughput for 802.11ac when other stations operating in 802.11a/n occupy

Manuscript received on March 10, 2016. This work is a follow-up of the invited journal to the accepted out-standing conference paper of the 18th International Conference on Advanced Communication Technology (ICACT2016).

Gul Zameen Khan is with the School of ICT, Griffith University, Australia. (corresponding author, phone: +61450039010, email: gz.khan@griffithuni.edu.au)

Dr. Ruben Gonzalez is a senior faculty member, head of Intelligent Wireless Technology and Applications research group, and director of the bachelor of computer science program at School of ICT, Griffith University, Australia. (email: r.gonzalez@griffith.edu.au).

Prof. Eun-Chan Park is with the Dept. of Information and Communication Engineering, Dongguk University, South Korea. (email: ecpark@dongguk.edu)

Dr. Xin-Wen Wu is with the School of ICT, Griffith University, Australia. (email: x.wu@griffith.edu.au)

the secondary channel. However, the simulation is performed in an ideal environment without taking into consideration the effects introduced by PHY and channel impairments.

Previous work addresses the individual features of 802.11ac. However, a comprehensive performance analysis of 802.11ac is important in order to estimate the achievable throughput. This paper extends our previous work [11] and considers several new features of 802.11ac (i.e., MCS, channel bandwidth, spatial stream) which can be a baseline to determine the system level throughput of an 802.11ac wireless network. To this end, a theoretical analysis based on both MAC and PHY layers is presented under a MIMO channel which is followed by simulation results. The paper thoroughly investigates the impacts of different features of 802.11ac on system throughput under different set of parameters. In addition, it provides a baseline model to measure the MAC and PHY layers performance of 802.11ac in terms of aggregate throughput. The impact of TGn channel models on the performance of 802.11ac is also presented for a complete networked system analysis of VHT.

The remainder of this paper is organized as follows: A brief overview of 802.11ac is discussed in section II. Section III describes a theoretical system model, MIMO channel model of 802.11ac and simulation set up. In Section IV, results and discussions are presented. Lastly, the paper is concluded in Section V.

II. Overview of IEEE 802.11ac

There are three key features that lead to VHT in 802.11ac. Each of them is described as follows:

A. More Spatial Streams(SS)

802.11ac has increased the number of SS from 4 in 802.11n up to 8 at PHY layer in MIMO Orthogonal Frequency Division Multiplexing (OFDM). There are three main advantages of using more MIMO in 802.11ac namely:

i. Extending the range
ii. Improving reliability
iii. Achieving higher throughput

In addition to SU-MIMO, 802.11 WAVE-2 also supports down link MU-MIMO in which an Access Point (AP) can send multiple data frames in the form of Aggregated MAC Protocol Data Unit (A-MPDU) to multiple receivers at the same time. In practice, the current 802.11ac devices support 3 SS and 4 SS in 802.11ac WAVE-1 and WAVE-2, respectively. However, a total of 8 SS can be supported in the upcoming products [1], [12].

B. Modulation and Coding

A more advanced modulation i.e. 256 QAM has been added to 802.11ac standard. This increases the number of bits per sub-carrier of OFDM compared to 64 QAM. As a result, the PHY data rate raises up to 33% as compared to previous 802.11 standards. On one hand it significantly increases data rate; on the other hand, however, it requires higher Signal to Noise Ratio (SNR) for receivers to correctly demodulate the symbols. Similarly, 802.11ac supports various coding rate of $\frac{1}{2}$, $\frac{2}{3}$, $\frac{3}{4}$, and $\frac{5}{6}$ [1].

C. Wider Channel Bandwidth

With 5 GHz band, the bandwidth of 802.11ac has been increased. In addition to 20 MHz and 40 MHs channels that were already available in 802.11n, wider channels of 80 MHz and 160 MHz have been added in 802.11ac. Furthermore the 160 MHz channel can be established with two contiguous or non-contiguous 80 MHz channels [1].

III. Simulation and Numerical Analysis

In this section we describe our system model for MAC and PHY layers and derive a theoretical formulation to calculate the performance of MAC and PHY layers numerically. We also formulate a MIMO channel model for 802.11ac and describe our simulation environment.

A. MAC Layer Theoretical Analysis

We consider a single hop fully connected Single Basic Service Set (BSS) with n Stations(STAs) and one AP. It is assumed that each STA can sense transmission from every other STA in the same BSS. All STAs operate in uplink saturated mode i.e., they always have data to send to the AP. A data transmission is considered successful if it is followed by an Acknowledgement (ACK) from the AP, otherwise it is retransmitted. The wireless channel is assumed ideal i.e., a frame is failed only due to collision that occurs when two or more STAs access the shared channel simultaneously.

We consider the Markov model of [13] that represents the Distributed Coordination Function (DCF) as two stochastic processes namely: $b(t)$ and $s(t)$ to model the backoff time counter and the backoff stage, respectively. Without the loss of generality, let CW_{min} and CW_{max} represent minimum and maximum contention windows, respectively. Let m indicates maximum backoff stage such that $CW_{max} = 2^m CW_{min}$. Let CW_i represents the contention window of a STA at ith backoff stage i.e., $CW_i = 2^i CW_{min}$ where $i \in [0, m]$. Thus $b(t)$ takes any random value from $[0, CW_i]$ where i is modelled by $s(t)$. For the sake of simplicity, we represent $CW_{min} = W$. The key approximation is that collision probability is constant regardless of retransmission stage. This is a reasonable approximation as long as W and n get larger.

During a randomly selected slot, a STA senses the channel in one of the three states namely: idle state (no transmission activities), busy due to successful transmission, or busy due to collision. Suppose a STA attempts to transmit a frame in a randomly chosen slot with probability τ. The system considers a Binary Exponential Backoff (BEB) mechanism which doubles the contention window on collision. If p represents the collision probability; then τ is given by [13]

$$\tau = \frac{2(1-p)}{(1-2p)(W-1) + pW(1-(2p)^m)} \tag{1}$$

The probability of collision p can be calculated from the fact that collision occurs if at least one of the remaining $n-1$ STAs starts transmission. Therefore, if $1-\tau$ is the probability that exactly one STA is idle then $(1-\tau)^{n-1}$ is the probability that $n-1$ STAs are idle. It follows that the probability that at least one of $n-1$ STAs transmits is given by [13]

$$p = 1 - (1-\tau)^{n-1} \quad (2)$$

Transmission probability τ and collision probability p can be calculated numerically by solving Eq. 1 and Eq. 2 using some numerical method (e.g., fixed point iteration). In addition, it can be proved that this system of non linear equations has a unique solution [13]. We have used Maple 15 [20] to solve Eq. 1 and Eq. 2.

We are interested in calculating throughput S of the system which is expressed as a ratio of average payload information transmitted in a slot per average duration of a slot.

$$S = \frac{E[D]}{E[T]} \quad (3)$$

where $E[D]$ is the expected value of data transmitted successfully in a randomly selected slot while $E[T]$ is the average length of a time slot;

$$E[D] = P_{tr} P_s E[L] \quad (4)$$

where P_{tr} denotes the probability that there is at least one transmission in the considered time slot. On the other hand, P_s is the probability that the given transmission is successful and $E[L]$ denotes the average length of payload data. Consequently, P_{tr} can be calculated for n contending stations as

$$P_{tr} = 1 - (1-\tau)^n \quad (5)$$

Similarly, P_s can be calculated from the fact that a transmission is successful if and only if exactly one STA transmits given that at least one STA transmits among n STAs, i.e.,

$$P_s = \frac{n\tau(1-\tau)^{n-1}}{1-(1-\tau)^n} \quad (6)$$

Accordingly, $E[D]$ is calculated from Eq. 5 and Eq. 6. In order to calculate $E[T]$, let us denote T as a random variable that indicates a randomly selected time slot. Moreover T takes any of the following three values:

$$T = \begin{cases} \sigma & \text{if the medium is idle} \\ T_s & \text{if successful transmission} \\ T_c & \text{if there is collision} \end{cases} \quad (7)$$

where σ is the duration of an empty slot while T_s and T_c are the average time when the channel is busy due to successful transmission and collision, respectively. The corresponding probability for these three cases can be calculated as

$$f_T(t) = \begin{cases} 1 - P_{tr} & \text{if } T = \sigma \\ P_{tr} P_s & \text{if } T = T_s \\ P_{tr}(1-P_s) & \text{if } T = T_c \end{cases} \quad (8)$$

Using Eq. 7 and Eq. 8, $E[T]$ can be calculated as

$$E[T] = \sum_{\forall t, T} T f_T(t) \quad (9)$$

Finally, the normalized throughput S is calculated by using Eq. 4 and Eq. 9 in Eq. 3. As far as T_s and T_c are concerned, they are calculated using PHY system model discussed in the following sub section.

TABLE I
802.11AC PHY FRAME

L-STF	L-LTF	L-SIG	VHT-SIG-A	VHT-STF	VHT-LTFs	VHT-SIG-B	Data

B. PHY Layer Theoretical Analysis

As discussed in Section II, the IEEE 802.11ac standard can increase throughput with the help of wider Radio Frequency (RF) channel bandwidth, more spatial streams, MU-MIMO, and advanced MCSs. The performance of PHY can be modelled by taking into account the aforementioned features. TABLE I shows a general format of a PHY layer frame [1].

Let T_x be the transmission time of a STA. We assume that the frame aggregation is not employed. Then, T_x can be derived as follows [1].

$$T_x = T_{LEG-PREAMBLE} + T_{L-SIG} + T_{VHT-SIG-A} + T_{VHT-PREAMBLE} + T_{VHT-SIG-B} + T_{DATA} \quad (10)$$

$$T_{LEG-PREAMBLE} = T_{L-STF} + T_{L-LTF} \quad (11)$$

$$T_{VHT-PREAMBLE} = T_{VHT-STF} + N_{VHTLTF} \times T_{VHT-LTF} \quad (12)$$

where T_{L-SIG}, $T_{VHT-SIG-A}$, $T_{VHT-SIG-B}$, T_{LTF}, T_{STF}, $T_{VHT-STF}$, $T_{VHT-LTF}$ are fields of PHY frame shown in TABLE II. N_{VHTLTF} shows the number of long training symbols which is determined from the number of space-time streams [14]. Similarly,

$$T_{DATA} = \begin{cases} N_{SYM} \times T_{SYM} & \text{for long GI} \\ T_{SYML} \lceil \frac{T_{SYMS} \times N_{SYM}}{T_{SYML}} \rceil & \text{for short GI} \end{cases} \quad (13)$$

where GI, T_{SYM}, T_{SYMS} and T_{SYML} indicate Guard Interval, symbol interval, short GI symbol interval, and long GI symbol interval, respectively. Their values are listed in TABLE II.

$$T_{SYM} = \begin{cases} T_{SYML} & \text{for long GI} \\ T_{SYMS} & \text{for short GI} \end{cases} \quad (14)$$

$$N_{SYM} = m_{STBC} \times \lceil \frac{M}{m_{STBC} \times N_{DBPSL}} \rceil \quad (15)$$

where $\lceil x \rceil$ = smallest integer $\geq x$ and N_{DBMS} indicates the number of data bits per symbol.

$$M = 8 \times APEP_{LENGTH} + N_{Service} + N_{tail} \times N_{ES} \quad (16)$$

$$m_{STBC} = \begin{cases} 2 & \text{if STBC is used} \\ 1 & \text{otherwise} \end{cases} \quad (17)$$

where $APEP_{LENGTH}$ indicates the final value of A-MPDU i.e., payload size and N_{ES} represents the number of Binary Convolution Code (BCC) encoders. The value of N_{ES} depends on the MCS and channel bandwidth and they are listed in TABLEs IV-VII. Space-Time Block Coding (STBC) is an encoding technique that greatly improves the reliability of communication in 802.11ac. T_x is calculated by using Eq. 11-14 in Eq. 10.

TABLE II
MAC AND PHY PARAMETERS

Parameter	Value	Para	Value	Para	Value
Slot time (σ)	9 μs	CW_{min}	16	T_{DIFS}	34 μs
L_{macH}	34 bits	CW_{max}	1024	T_{SIFS}	16 μs
$T_{VHT-STF}$	4 μs	T_{SYMS}	3.6 μs	T_{STF}	8 μs
$T_{VHT-SIG-A}$	8 μs	T_{L-SIG}	4 μs	T_{LTF}	8 μs
$T_{VHT-SIG-B}$	4 μs	T_{SYML}	4 μs	N_{tail}	6 bits
$T_{VHT-LTF}$	4 μs	$N_{service}$	16 bits	ρ	1 μs

Now, we calculate successful transmission time (T_s) and collision time (T_c) for basic DCF i.e., without Ready To Send (RTS)/Clear To Send (CTS).

$$T_s = T_{DIFS} + T_x + \rho + T_{SIFS} + T_{ACK} + \rho$$

$$T_c = T_{DIFS} + T_x + \rho + T_{ACK-TOut}$$

where T_{DIFS}, T_{SIFS}, T_{ACK}, and ρ indicate DCF Inter-Frame Spacing time, Short Inter-Frame Spacing time, transmission time of ACK frame and propagation delay of 802.11ac frame, respectively. Their values are listed in TABLE II. Similarly, $T_{ACK-TOut}$ represents the time out for ACK frame and is calculated as

$$T_{ACK-TOut} = T_{ACK} + T_{SIFS} + \rho$$

The T_s and T_c for DCF with RTS/CTS can be determined in a similar way.

C. Channel Model for 802.11ac

In order to evaluate the impact of the channel on MAC and PHY layers of 802.11ac, we consider a set of channel models that are designed for IEEE 802.11 WLAN [15]. Each model is applicable to a specific environment with a set of 6 profiles, labelled A to F. All these profiles cover different scenarios as listed in TABLE III. Each channel model has a path loss model including shadowing, and a MIMO multipath fading model, which describes the multipath delay profile, the spatial properties, the K-factor distribution shown as Rician K-factor in TABLE III, and the Doppler spectrum.

Each channel model has a certain number of taps which are associated with specific delays. Furthermore, each channel model is comprised of a certain number of clusters. A cluster is made up of a set of taps. The number of taps, Root Mean Square (RMS) delay (σ_{RMS}), maximum delay (σ_{Max}), the number of clusters and standard deviation of shadow fading both in case of Line of Sight (LOS) and Non Line of Sight (NLOS) for each model are listed in TABLE III. The LOS K-factor is applicable only to the first tap while all the other taps K-factor remain at $-\infty$ dB.

A set of spatial properties are defined for each cluster:

i. Mean Angle of Arrival (AoA)
ii. Mean Angle of Departure (AoD)
iii. Angular Spread (AS) at transmitter
iv. AS at receiver

These parameters determine the transmit and receive correlation matrices associated with each tap delay. The LOS component can only be present on the 1st tap. If the distance between the transmitter and the receiver is greater than d_{BP} then LOS component is not present. Note that d_{BP} is the break-point distance or distance of first wall (i.e., distance of transmitter from the first reflector). The d_{BP} for all channel models (A-F) are listed in 5th column of TABLE III.

We consider a path loss model that takes into account the free space loss L_{FS} (log-distance model with the path-loss exponent of 2) up to d_{BP} and log-distance model with the path-loss exponent of 3.5 after d_{BP} [16]. For each of the models, a different break-point distance d_{BP} was chosen.

$$L(d) = \begin{cases} L_{FS}(d) & \text{if } d \leq d_{BP} \\ L_{FS}(d_{BP}) + 35log10(d/d_{BP}) & \text{if } d > d_{BP} \end{cases} \quad (18)$$

where d is the distance between transmitter and receiver. The other parameters of the path loss model are listed of TABLE III. The standard deviations of log-normal (Gaussian in dB) shadow fading are also included in 10th column in TABLE III. The values were found to be in the range between 3 and 14 dB [17].

Similarly, the zero-mean Gaussian probability distribution is given by

$$p(x) = \frac{1}{\sqrt{2\pi\sigma}} e^{[\frac{x^2}{2\sigma^2}]} \quad (19)$$

We are interested in modelling the MIMO channel of 802.11ac. Thus the correlation between transmit and receive antenna is an important aspect of the MIMO channel. To this end, we follow a procedure based on the transmitter and receiver correlation matrices [18] to calculate the MIMO channel matrix H for each tap, at one instance of time, in the A-F delay profile models. The channel matrix H is derived as a sum of two matrices namely: a fixed LOS matrix with constant entries, and a Ryleigh NLOS matrix with variable entries as follows

$$H = \sqrt{P} \left(\sqrt{\frac{K}{K+1}} H_F + \frac{1}{K+1} H_V \right) \quad (20)$$

where P shows the power of each tap which is obtained by summing all the power of LOS and NLOS powers, and K is the Ricean K-factor. Eq. 20 can be expressed for any number of transmitter and receiver for MIMO. If there are T input antennas at the transmitter and R output antennas at the receiver then H_F and H_V in Eq. 20 can be represented as

$$H_F = \begin{bmatrix} e^{j\phi_{11}} & e^{j\phi_{12}} & \dots & e^{j\phi_{1T}} \\ e^{j\phi_{21}} & e^{j\phi_{22}} & \dots & e^{j\phi_{2T}} \\ \vdots & \vdots & \ddots & \vdots \\ e^{j\phi_{R1}} & e^{j\phi_{R2}} & \dots & e^{j\phi_{RT}} \end{bmatrix}$$

$$H_V = \begin{bmatrix} X_{11} & X_{12} & \dots & X_{1T} \\ X_{21} & X_{22} & \dots & X_{2T} \\ \vdots & \vdots & \ddots & \vdots \\ X_{R1} & X_{R2} & \dots & X_{RT} \end{bmatrix}$$

where $e^{j\phi_{ij}}$ shows the constant elements of LOS matrix H_F and X_{ij} represents the element of variable NLOS Rayleigh matrix H_V between i^{th} receiving and j^{th} transmitting antenna.

TABLE III
PARAMETERS OF A-F PATHLOSS CHANNEL MODELS 802.11AC

Channel name	User case scenario	Conditions	K (dB)	D_{BP}(m)	No of taps	σ_{RMS}	σ_{Max}	No of clusters	Shadow fading std. dev. (dB) before/after d_{BP} (LOS/NLOS)
A	Flat Fading	LOS	0	5	1	0	0	1	3
		NLOS	$-\infty$						4
B	Residential	LOS	0	5	9	15	80	2	3
		NLOS	$-\infty$						4
C	Residential/ small office	LOS	0	5	14	30	200	2	3
		NLOS	$-\infty$						4
D	Typical office	LOS	3	10	18	50	390	3	3
		NLOS	$-\infty$						6
E	Large office	LOS	6	20	18	100	730	4	3
		NLOS	$-\infty$						6
F	Large space indoors and outdoors	LOS	6	30	18	150	1050	6	3
		NLOS	$-\infty$						6

It is assumed that X_{ij} is a complex Gaussian random variable with zero mean and unit variance.

In order to correlate the X_{ij} elements of the matrix H_V, the following method is used

$$[X] = [R_{rx}]^{\frac{1}{2}}[H_{iid}][R_{tx}]^{\frac{1}{2}} \tag{21}$$

where R_{rx} and R_{tx} are the receive and transmit correlation matrices, respectively, and H_{iid} is a complex Gaussian random variable. All these Gaussian random variables are supposed to be identically independent with zero mean and unit variance. In addition, R_{tx} and R_{rx} are given by

$$[R_{tx}] = [\rho_{txij}] \tag{22}$$

$$[R_{rx}] = [\rho_{rxij}] \tag{23}$$

where ρ_{txij} are the complex correlation coefficients between i^{th} and j^{th} transmitting antennas, and ρ_{rxij} are the complex correlation coefficients between i^{th} and j^{th} receiving antennas.

Alternatively, we use another approach i.e., Kronecker product of the transmit and receive correlation matrices to calculate X [18].

$$[X] = ([R_{tx}] \otimes [R_{rx}])^{\frac{1}{2}}[H_{iid}] \tag{24}$$

It can be seen that H_{iid} is an array in this case instead of matrix. The R_{tx} and R_{rx} matrices are given as:

$$R_{tx} = \begin{bmatrix} 1 & {\rho_{tx12}}^{*} & \cdots & {\rho_{tx1T}}^{*} \\ \rho_{tx21} & 1 & \cdots & {\rho_{tx2T}}^{*} \\ \vdots & \vdots & \ddots & \vdots \\ \rho_{txR1} & \rho_{txR2} & \cdots & 1 \end{bmatrix}$$

$$R_{rx} = \begin{bmatrix} 1 & {\rho_{rx12}}^{*} & \cdots & {\rho_{rx1T}}^{*} \\ \rho_{rx21} & 1 & \cdots & {\rho_{rx2T}}^{*} \\ \vdots & \vdots & \ddots & \vdots \\ \rho_{rxR1} & \rho_{rxR2} & \cdots & 1 \end{bmatrix}$$

The values of complex correlation coefficient ρ are calculated from power angular spectrum (PAS), AS, mean AoA, mean AoD and individual tap powers [15], [19]. Consequently, for the Uniform Linear Array (ULA), the complex correlation coefficient at the linear antenna array is expressed as

$$\rho = R_{XX}(D) + jR_{XY}(D) \tag{25}$$

where $D = 2\pi d/\lambda$ (λ shows the wavelength in metre) , and R_{XX} and R_{XY} are the cross-correlation functions between the real parts and between the real part and imaginary part, respectively, with

$$R_{XX}(D) = \int_{-\pi}^{\pi} \cos(D \sin\phi) PAS(\phi) d\phi \tag{26}$$

$$R_{XY}(D) = \int_{-\pi}^{\pi} \sin(D \cos\phi) PAS(\phi) d\phi \tag{27}$$

We calculate the correlation coefficients matrices in three ways namely: uniform, truncated Gaussian, and truncated Laplacian PAS shapes [15].

D. Simulation Environment

We have implemented MAC and PHY layers of 802.11ac in matlab with given parameters as defined in [1]. TABLE II-VII list the parameters that are used in our theoretical analysis as well as simulation setup. We do not consider the frame aggregation scheme for the sake of simplicity. To simulate different features of PHY, we summarize the MCSs into four tables i.e., TABLES IV-VII for 20 MHz, 40 MHz, 80 MHz, and 160 MHz channels, respectively. The values of MCSs are chosen such that we cover maximum modulation and coding schemes.

We consider various modulation schemes namely: Quadrature Phase Shift Keying (QPSK), 16-QAM (Quadrature Amplitude Modulation), 64-QAM, and 256-QAM. The coding rate (R) is chosen as $\frac{1}{2}$, $\frac{2}{3}$, $\frac{3}{4}$, and $\frac{5}{6}$. In the same way, the number of SS (N_{SS}) is selected to be 1, 2, 4, and 8. The data rate is calculated from Eq. 13 whereas ACK rate is fixed at basic rate. We have run each simulation 20 times and have calculated average values to show stable results.

In order to implement a TGn channel in matlab, we use the parameters from TABLE III. In addition, we use OFDM with MIMO channel at our transmitter and receiver for our PHY and channel analysis of 802.11ac.

TABLE IV
MCS FOR 20 MHZ CHANNEL

MCS	Modulation	R	N_{ss}	N_{DBPS}	N_{ES}	Data rate (Mbps) 800 ns GI	400 ns GI
1	QPSK	1/2	1	52	1	13	14.4
			4	208	1	52	57.8
			8	416	1	104	115.6
3	16-QAM	1/2	1	104	1	26	28.9
			4	416	1	104	115.6
			8	832	1	208	231.1
5	64-QAM	2/3	1	208	1	52	57.8
6	64-QAM	3/4	1	234	1	58.5	65
7	64-QAM	5/6	1	260	1	65	72
8	256-QAM	3/4	1	312	1	78	86.7

TABLE V
MCS FOR 40 MHZ CHANNEL

MCS	Modulation	R	N_{ss}	N_{DBPS}	N_{ES}	Data rate (Mbps) 800 ns GI	400 ns GI
1	QPSK	1/2	1	108	1	27	30
			2	216	1	54	60
			4	432	1	108	120
			8	864	1	216	240
3	16-QAM	1/2	1	216	1	54	60
			2	432	1	108	120
			4	864	1	216	240
			8	1728	1	432	480
5	64-QAM	2/3	1	432	1	108	120
9	256-QAM	5/6	1	720	1	180	200

TABLE VI
MCS FOR 80 MHZ CHANNEL

MCS	Modulation	R	N_{ss}	N_{DBPS}	N_{ES}	Data rate (Mbps) 800 ns GI	400 ns GI
1	QPSK	1/2	1	234	1	58.5	65
			4	936	1	234	260
			8	1872	1	468	520
3	16-QAM	1/2	1	468	1	117	130
			4	1872	1	468	520
			8	3744	2	936	1040
5	64-QAM	2/3	1	936	1	234	260
8	256-QAM	3/4	1	1404	1	351	390
			4	5616	3	1404	1560
			8	11232	6	2808	3120

TABLE VII
MCS FOR 160 MHZ CHANNEL

MCS	Modulation	R	N_{ss}	N_{DBPS}	N_{ES}	Data rate (Mbps) 800 ns GI	400 ns GI
1	QPSK	1/2	1	468	1	117	130
			4	1872	1	468	520
			8	3744	2	936	1040
3	16-QAM	1/2	1	936	1	234	260
4	16-QAM	3/4	1	1404	1	351	390
5	64-QAM	2/3	1	1872	1	568	520
			4	7488	4	1872	2080
			8	14976	8	3744	4160
8	256-QAM	3/4	1	2808	2	702	780
			4	11232	6	2808	3120
			8	22464	12	5616	6240

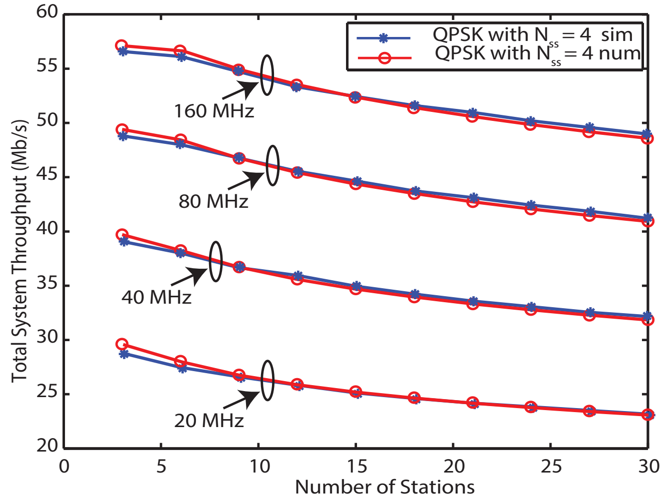

Fig. 1. Throughput for different channels as a function of number of STAs

IV. RESULTS AND DISCUSSIONS

We calculate aggregate throughput for different number of STAs and payload size.

A. Wider Channels

In order to evaluate the effect of wider channels on system throughput, we calculate total throughput for 20 MHz, 40 MHz, 80 MHz, and 160 MHz channels. We simulate a case that uses QPSK with $N_{ss} = 4$, and $GI = 400\ ns$. The payload size is fixed at 1500 bytes. As shown in Fig. 1, the total throughput decreases for the all cases of channel bandwidths as the number of STAs increases. However, the total throughput increases with respect to the increase of channel bandwidth. Compared to the case of 20 MHz channel bandwidth, the total throughput is increased by more than 10, 20, and 30 Mb/s in the cases of 40, 80, and 160 MHz channel bandwidth, respectively. It is important to note that the increase of total throughput is not proportional to the increase of channel bandwidth, i.e., less than one quarter increase of channel bandwidth. The theoretical (num) results also show a similar trend.

In a similar way, we observe the effects of available channel bandwidth on throughput as a function of payload size. For this purpose, we use a modulation of 16 QAM with one SS i.e., $N_{ss} = 1$, and $GI = 800\ ns$. In the case of 20/40/80/160 MHz channel, the coding rate of 16QAM can be 1/2 or 3/4 (see Table IV-VII). The number of STAs is 20 (i.e., $n = 20$) in this set up. Fig. 2 illustrates that total throughput increases by nearly 10 Mbps as the channel width is doubled.

B. Modulation

The choice of a particular modulation scheme can greatly affect the system throughput. To observe this result, we fix the number of SS to 1 in a 20 MHz channel with $GI = 800\ ns$ and payload size of 1500 bytes. We calculate throughput for different modulation schemes. As illustrated in Fig. 3, QPSK gives the lowest throughput while 256 QAM produces the

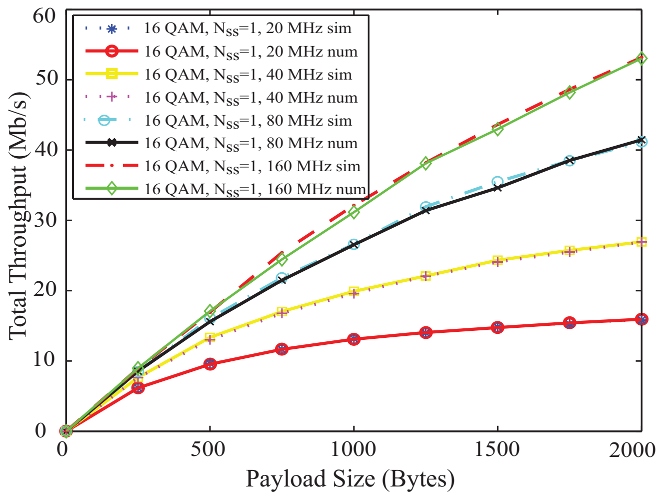

Fig. 2. The effects of wider channels on throughput for different payload size

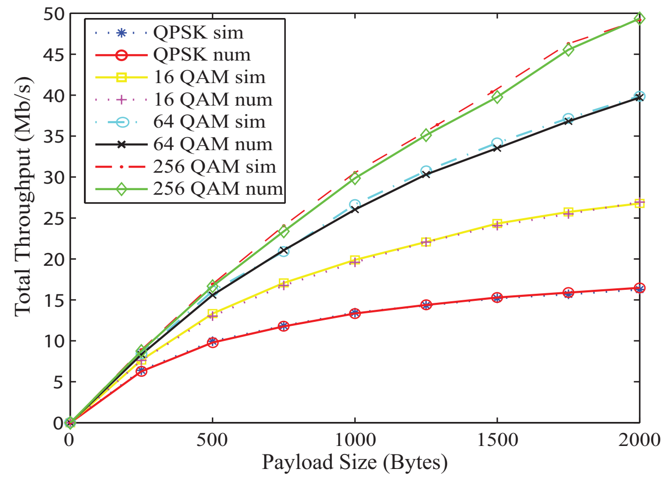

Fig. 4. Throughput for different modulations as a function of payload size

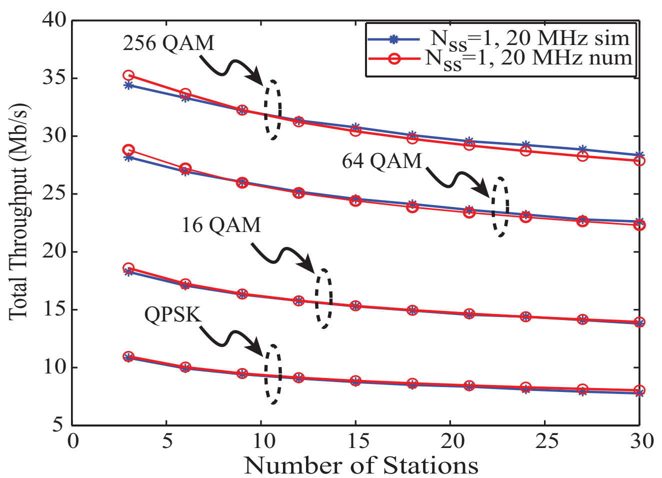

Fig. 3. Throughput of different modulation schemes for different STAs

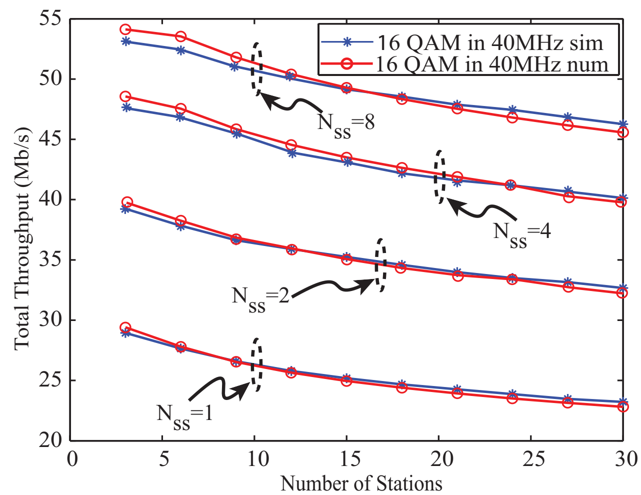

Fig. 5. The effects of SS on throughput for different number of STAs

highest total throughput. The improvement is 20 Mpbs from QPSK to 256 QAM.

It is also worth noting that total throughput is greatly affected by different modulation techniques under different payload sizes. To notice this fact, the number of STAs is fixed to 20 while $N_{ss} = 1$ with QPSK in a 40 MHz channel and $GI = 800\ ns$. Fig. 4 represents that the total throughput increases as the payload size is increased. In addition, the higher order modulation schemes produce higher throughput. The difference of throughput between different modulation schemes is increased with increase in payload size. For instance, when payload size reaches 2000 bytes, there is an elevation of 10 Mbps for each modulation scheme (i.e., QPSK, 16 QAM, 64 QAM and 256 QAM).

C. Multiple Spatial Streams

Now, we focus on the effects of different number of transmitting antennas on total throughput. We consider a case of 16 QAM with 40 MHz channel, $GI = 800\ ns$ and fixed payload size of 1500 bytes. Although 802.11ac may support 1 to 8 SSs, however, for the sake of simplicity and comprehension, we consider $N_{ss} = \{1, 2, 4, 8\}$. The results are depicted in Fig. 5. It is clear that the total throughput decreases as we increase the number of STAs for all SSs. Nonetheless, the overall throughput for a particular number of SS increases by 10 Mbps as the number of SS is doubled. In the same manner, Fig. 6 represents the total throughput for different antenna streams. The modulation used is QPSK with $GI = 800\ ns$ in 40 MHz channel. The number of STAs is once again fixed at 20. As can be seen in Fig. 6, the total throughput increases as we increase the payload size. In particular, the total throughput increases by almost 10 Mbps for every $2N_{ss}$.

D. Coding Rate

The relationship between total throughput and different number of STAs is examined under various coding rate i.e., $R = \{\frac{2}{3}, \frac{3}{4}, \frac{5}{6}\}$. The other parameters are set as $N_{ss} = 1$, modulation = 64 QAM, and $GI = 400\ ns$ in 20 MHz channel. Fig. 7 shows that the total system throughput increases by 1

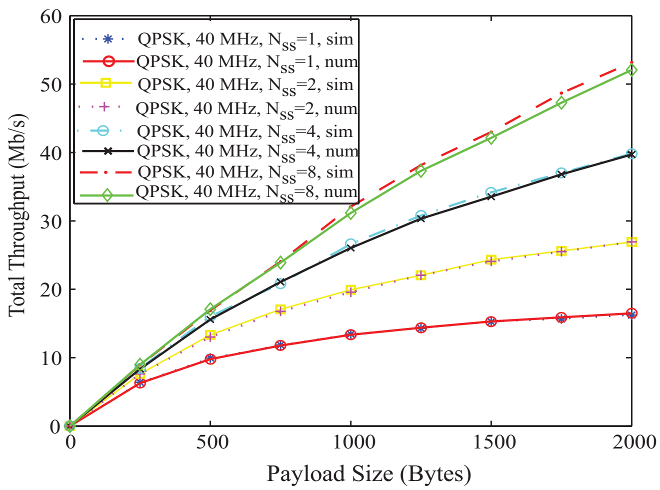

Fig. 6. Throughput for different antenna streams with variable payload size

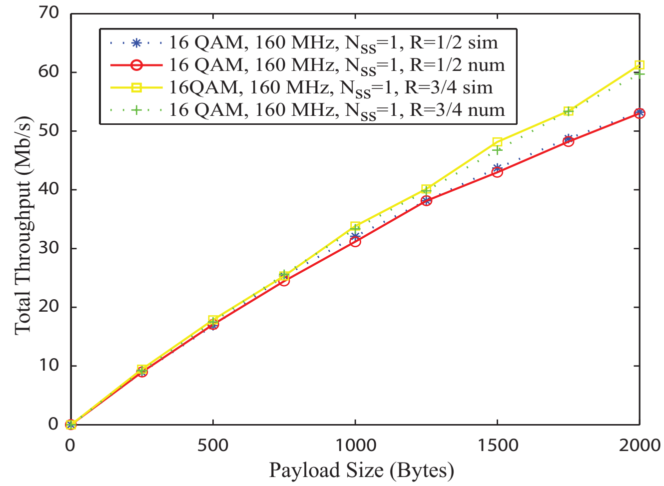

Fig. 8. Throughput of different coding rate for different payload

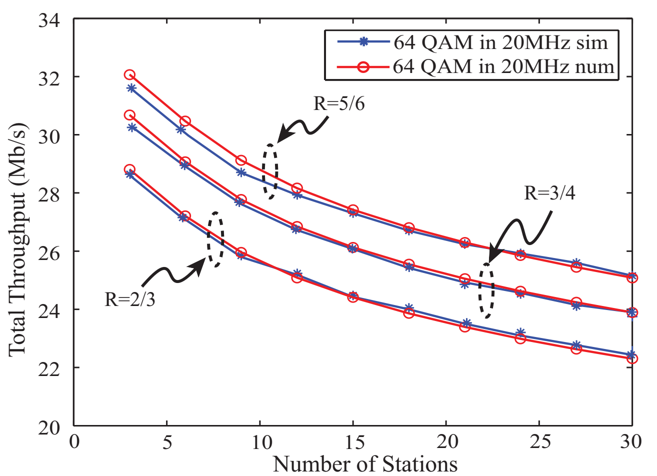

Fig. 7. Throughput in different coding rate (R) for different STAs

Mbps as we move to the next available coding rate under the aforementioned setup.

The influence of coding rate on total throughput as a function of payload size is illustrated in Fig. 8. We choose 16 QAM in 160 MHz channel with $N_{ss} = 1$. The number of STAs is 20 while $GI = 800ns$. The total throughput increase by 4 Mbps for $R = \frac{3}{4}$ than $R = \frac{1}{2}$ when the payload size is 1500. However, the throughput rise reaches upto 9 Mbps for $R = \frac{3}{4}$ than $R = \frac{1}{2}$ as payload size is increased to 2000 bytes. Fig. 8 indicates that coding rate can tremendously affect total throughput under variable frame size.

E. Analysis under TGn Channel

As illustrated in TABLE III, each TGn channel has a different profile. In order to investigate the impact of a channel on MCS, we simulate 802.11ac under channel D and see the performance in terms of Symbol Error Rate (SER). For this purpose, we use an OFDM system under a 40 MHz MIMO multipath Rayleigh fading channel. Accordingly, a 128 point Fast Fourier Transform (FFT) is used with 128 subcarriers for 40 MHz.The bandwidth of each sub carrier is 312.5 KHz for OFDM in 802.11ac. Out of 124 subcarriers, the 114 subcarriers (-58 to 2 and 2 to 58) are used for data and pilot (timing and synchronization). The indices used for pilot subcarriers are -53, -25, -11, 11, 25, and 53. Subcarriers -1, 0, -1 are used as DC while the remaining 11 subcarriers are used as left (6) and right (5) guard bands.

The SER of the system is calculated for BPSK, QPSK, 16-QAM, 64-QAM and 256-QAM under different Energy per Symbol (E_s/N_o) for OFDM transceiver under 40 MHz 2x2 MIMO TGn D channel as shown in Fig. 9. The SER decreases as E_s/N_o increases for all modulation schemes. However, in lower E_s/N_o, the SER of BPSK is much lower as compared to other modulation schemes. Similarly, QPSK shows lower SER at higher noise as compared to other high order modulation schemes. A similar trend can be seen for 16-QAM and 64-QAM as compared to 256-QAM. Thus in an error-prone channel conditions, 802.11ac suffers from almost 50% SER for 256-QAM as compared to BPSK.

Next, we consider the impact of all TGn channels i.e., (A to F) TABLE III on the performance of 802.11ac network. For this purpose, we fix all other parameters except the number of of transmit and receive antennas. This will give us an idea of how 1x1, 2x1, and 4x4 MIMO changes the performance of 802.11ac network under different TGn channels. We use the MIMO OFDM system with 64 point FFT, 20 MHz channel, 64-QAM, coding rate of 1/2 (i.e., MCS = 3) as illustrated in TABLE IV. The packet length is set to 1500 bytes. We calculate the Packet Error Rate (PER) to estimate the performance of MIMO OFDM 802.11ac under different channels. We sent 1000 packets for each Signal to Noise Ratio (SNR) point that ranges from 0 dB to 50 dB. The distance between transmitter and receiver is set to 10 m. We also add Additive White Gussian Noise (AWGN) in order to make a realistic estimation of wireless environment.

We observe that the PER and SNR can be divided into three different levels when the SNR of channel is changed from 0 dB to 50 dB for all the 6 channel models in 1x1, 2x2 and 4x4 MIMOs. This trend can be seen in different configurations of transmit and receive antennas as shown in Fig. 10-15. Let us

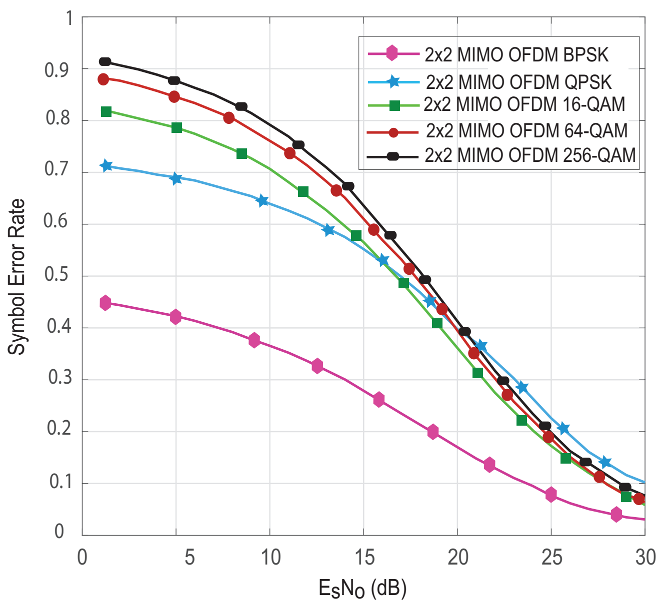

Fig. 9. Symbol Error Rate vs. EsNo for different Modulation schemes

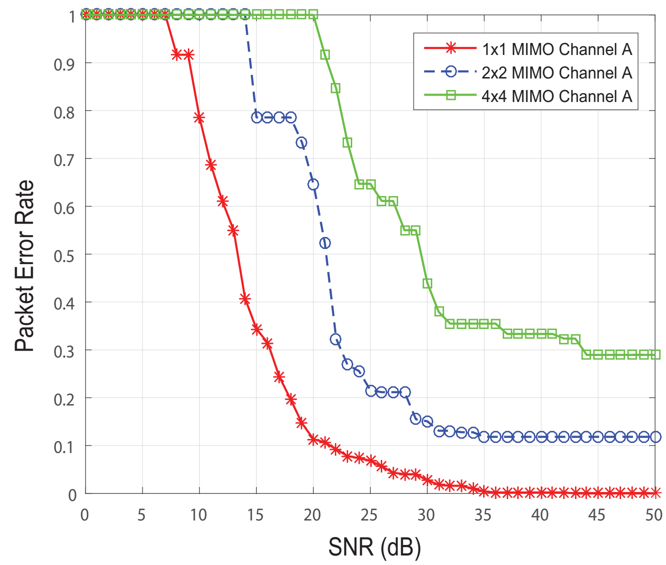

Fig. 10. Packet Error Rate vs. SNR of Channel A under different MIMO configurations

call these three levels as *initial level*, *intermediate level*, and *final level*. The PER is explained with the help of Fig. 10-15 and TABLE VIII-X. As shown in Fig. 10-15 and TABLE VIII-X, the PER remains constant at *initial* and *final levels* while it drops down over a range of SNR values at *intermediate level* for all the channel models under 1x1, 2x2 and 4x4 MIMOs. The range of SNR values for the three levels changes differently for the 6 channel models under different MIMO configurations.

As illustrated in TABLE VIII-X, the PER is 100% at *initial level* for all the channels and all cases. Thus the system performance is worst at *initial level*. However, the range of SNR points at *initial value* increases as we increase the number of transmit and receive antennas. For example: the average range of SNR (average of A-F) is 0 to 9.6 dB (TABLE VIII) , 0 to 14.3 dB (TABLE IX), and 0 to 20.1 dB (TABLE X) for 1x1, 2x2, and 3x3 MIMOs, respectively. It shows that the performance of 1x1 MIMO is better than that of 2x2 MIMO and 4x4 MIMO. Similarly, the performance of 2x2 MIMO is better than that of 4x4 MIMO in terms of packet reception at lower SNR values. In the same way, the PER remains constant at *final level* for all channel models and all MIMO configuration. However, the values of PER and the range of SNR are different for different channels under different MIMOs. For example at *final level*, the PER and SNR of channel model A remains 0%, 11.82%, and 28.94% at 35-50 dB, 35-50 dB, and 44-50 dB for 1x1 MIMO, 2x2 MIMO, and 4x4 MIMO configurations, respectively. A similar trend can be found for other channels. On the other hand for *intermediate level*, the PER drops down from higher values to lower values over a range of SNR points. The slop and trend of each drop is different for different channel models and different MIMO configurations.

Based on our simulation results, we find interesting performance patterns for 802.11ac under different channel models. As shown in Fig. 10-15 and TABLE VIII, the PER of 802.11ac is 100% at *initial level* and 0% *final level* for channel models A, B, and C under 1x1 MIMO. The PER is 2% and 6% for channel models D and E, respectively. However, the PER is 11.70% in case of channel model F which is the worst performance for 1x1 MIMO for a given configurations.

Similarly, under 2x2 MIMO, the system performs best for channel models B, C and D where the PER remains at 2% at *final level* for these three channel models as shown in Fig. 10-15 and TABLE IX. However, the system performance degrades to some extent for channel models A, E, and F where the PER is 11.82%, 6.1%, and 18.03%, respectively. The PER for channel model F is the maximum (18.03%) as compared to other models. Channel model B relatively provides the best results under 2x2 MIMO as shown in Fig. 10-15.

The PER of 802.11ac network remains lower for channel models B, C, and D under 4x4 MIMO as illustrated in Fig. 10-15 and TABLE X. In this case, the performance is worst for channel model A where PER remains 28.94% at *final level*. The system achieves relatively the best performance for channel model D as compared to the other channel models under 4x4 MIMO configuration. This can be seen in TABLE X where the PER is 0%, 84.61%-0.26%, and 0.20% for *initial*, *intermediate*, and *final levels*, respectively.

V. Conclusion

This paper investigated the performance of 802.11ac in terms of system throughput under its several new key features. A theoretical model was presented that is based on MAC and PHY layer parameters. It was shown through simulation and theoretical analysis that the choice of a particular modulation and coding scheme, number of spatial streams, and channel size can greatly affect the total throughput of system. A MIMO multipath fading channel model was formulated to further investigate the effects of new features of 802.11ac. Although 802.11ac increases throughput many fold due to high-order

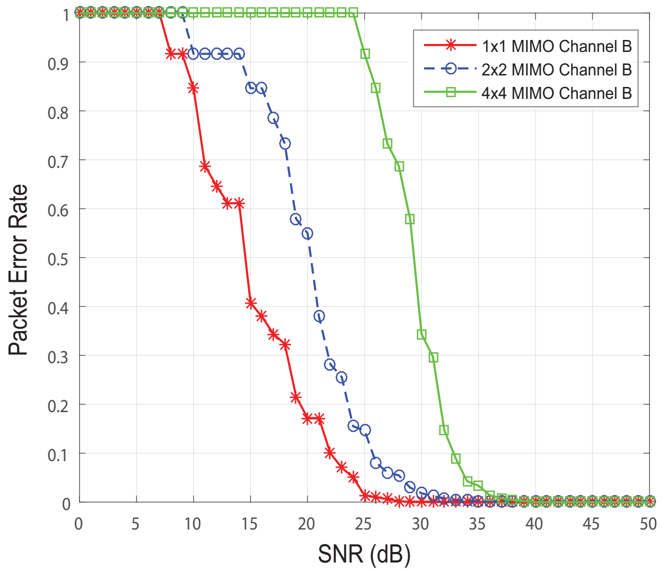

Fig. 11. Packet Error Rate vs. SNR of Channel B under different MIMO configurations

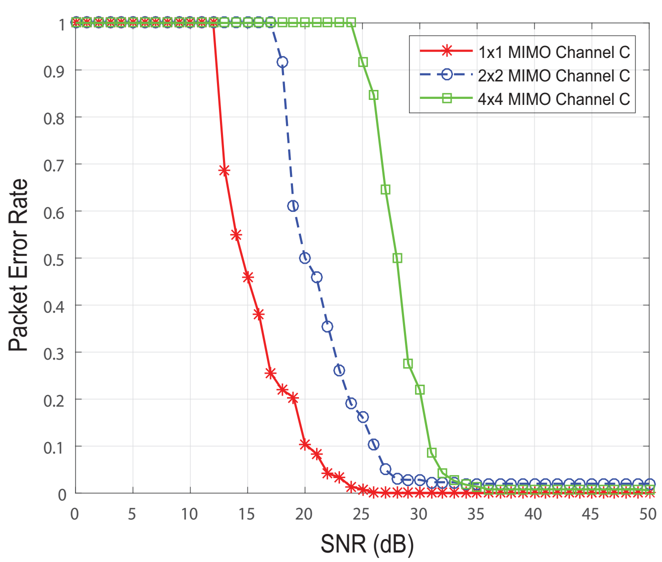

Fig. 12. Packet Error Rate vs. SNR of Channel C under different MIMO configurations

TABLE VIII
PER LEVELS FOR A RANGE OF SNR OF 1X1 MIMO-OFDM 802.11AC WLAN SYSTEM

Channel model	Parameter name	Initial level	Intermediate level	Final level
A	SNR (dB)	0-7	8-34	35-50
	PER (%)	100	91.66-2	0
B	SNR (dB)	0-7	8-25	26-50
	PER (%)	100	91.66-2	0
C	SNR (dB)	0-13	14-26	27-50
	PER (%)	100	68.75-2	0
D	SNR (dB)	0-7	8-25	26-50
	PER (%)	100	91.66-8	6
E	SNR (dB)	0-11	12-40	41-50
	PER (%)	100	91.66-3.2	2
F	SNR (dB)	0-13	14-20	21-50
	PER (%)	100	68.75-14.10	11.70

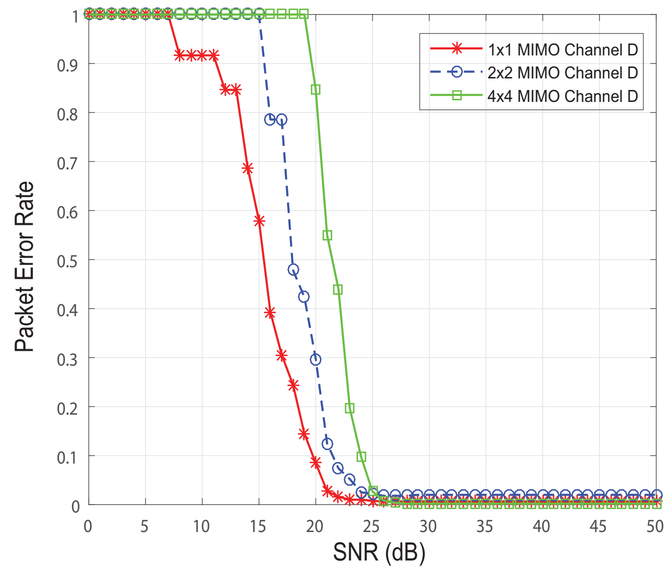

Fig. 13. Packet Error Rate vs. SNR of Channel D under different MIMO configurations

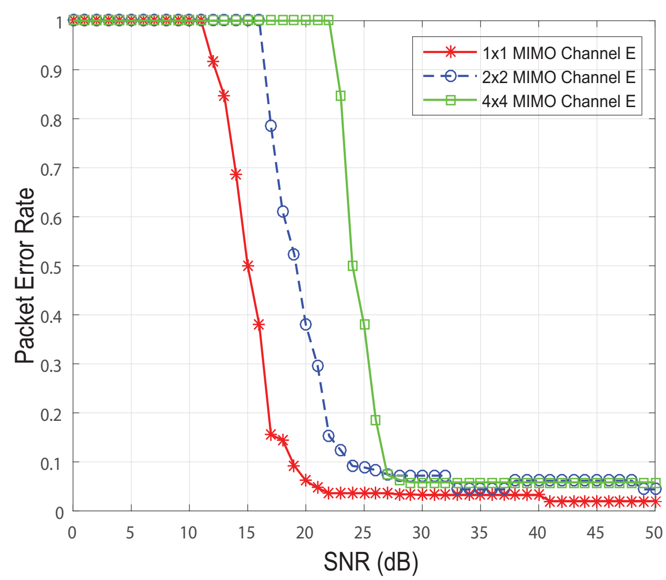

Fig. 14. Packet Error Rate vs. SNR of Channel E under different MIMO configurations

TABLE IX
PER LEVELS FOR A RANGE OF SNR OF 2X2 MIMO-OFDM 802.11AC WLAN SYSTEM

Channel model	Parameter name	Initial level	Intermediate level	Final level
A	SNR (dB)	0-14	15-34	35-50
	PER (%)	100	78.57-12.79	11.82
B	SNR (dB)	0-9	10-34	35-50
	PER (%)	100	91.66-4	2
C	SNR (dB)	0-17	18-33	34-50
	PER (%)	100	91.66-2.32	2
D	SNR (dB)	0-15	16-28	29-50
	PER (%)	100	78.57-1.8	2
E	SNR (dB)	0-16	17-36	37-50
	PER (%)	100	78.57-3.4	6.1
F	SNR (dB)	0-15	16-33	34-50
	PER (%)	100	91.66-19.29	18.03

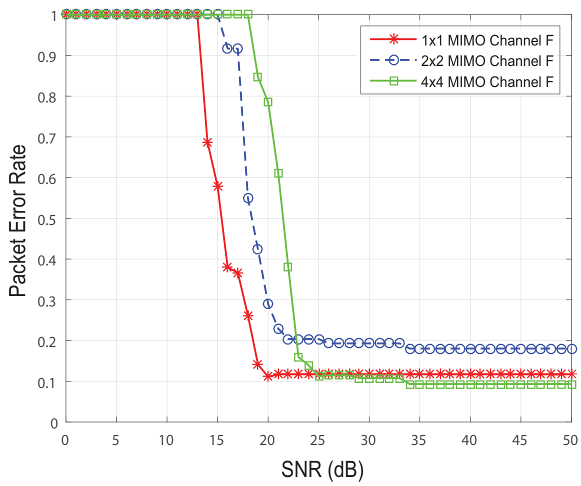

Fig. 15. Packet Error Rate vs. SNR of Channel F under different MIMO configurations

TABLE X
PER LEVELS FOR A RANGE OF SNR OF 4X4 MIMO-OFDM 802.11AC WLAN SYSTEM

Channel model	Parameter name	Initial level	Intermediate level	Final level
A	SNR (dB)	0-20	21-43	44-50
	PER (%)	100	91.66-32.35	28.94
B	SNR (dB)	0-24	25-35	36-50
	PER (%)	100	91.66-4.2	0
C	SNR (dB)	0-24	25-35	36-50
	PER (%)	100	91.66-1	0.8
D	SNR (dB)	0-19	20-27	28-50
	PER (%)	100	84.61-0.26	0.20
E	SNR (dB)	0-16	17-28	29-50
	PER (%)	100	84.61-6.3	5.8
F	SNR (dB)	0-18	19-33	34-50
	PER (%)	100	84.61-10.78	9.32

modulation scheme, more bandwidth and spatial streams, the performance can also be degraded drastically in an error-prone channel. We also investigated the performance of 802.11ac under different TGn channel models to find the performance patterns of different channel models.

REFERENCES

[1] *IEEE 802.11ac-Enhancements for Very High Throughput for operation in bands below 6 GHz*, IEEE P802.11ac/D5.0, 2013.

[2] Wi-Fi Alliance, *Wi-Fi certified products finder.*[Online]. Available:https://www.wi-fi.org/product-finder

[3] V. Jones, H. Sampath, "Emerging technologies for WLAN," *IEEE Communications Magazine*, vol. 53, no.3, pp. 141–149, March 2015.

[4] *IEEE 802.11n-Part 11: Wireless LAN Medium Access Control (MAC) and Physical Layer (PHY) Specifications: Enhancements for Higher Throughput,* IEEE 802.11n-2009.

[5] Z. Yunze, P.H. Pathak, and P. Mohapatra, "A first look at 802.11ac in action: Energy efficiency and interference characterization," *IFIP Networking 2014 Conf.*, 2-4 June 2014, pp. 1–9.

[6] E. H. Ong et al., "IEEE 802.11ac: Enhancements for very high throughput WLANs," *Proc. IEEE PIMRC*, Sep. 2011, pp. 849-853.

[7] C. Zhu et al., "Mac enhancements for downlink multi-user mimo transmission in next generation wlan," *IEEE Consumer Communications and Networking Conf. (CCNC),* Jan. 2012, pp. 832–837.

[8] Timo Vanhatupa, *Wi-Fi Capacity Analysis for 802.11 ac and 802.11 n: Theory and Practice,* Ekahau Inc., 2013.

[9] Oran Sharon, Yaron Alpert, "MAC level Throughput comparison: 802.11ac vs. 802.11n," *Physical Communication,* vol. 12, September 2014, pp. 33-49.

[10] Minyoung Park, "IEEE 802.11ac: Dynamic Bandwidth Channel Access,"in *IEEE International Conference on Communications (ICC) 2011*, pp.1-5, 5-9 June 2011.

[11] Gul Zameen Khan, Ruben Gonzalez, Eun-Chan Park, "A performance analysis of MAC and PHY layers in IEEE 802.11ac wireless network," in *18th International Conference on Advanced Communication Technology (ICACT)*, Pyeongchang Kwangwoon Do, South Korea, pp.20-25, 31 Jan - 3 Feb 2016.

[12] Aruba Networks, *802.11ac In-Depth.*[Online]. Available: http://www.arubanetworks.com/pdf/technology/whitepapers/WP_80211acInDepth.pdf

[13] G. Bianchi, "Performance analysis of the IEEE 802.11 distributed coordination function,"*IEEE J. Sel. Areas Commun.,* vol. 18, no.3, pp. 535–547, March 2000.

[14] Yong Soo Cho, et al., *MIMO-OFDM wireless communications with MATLAB,* John Wiley and Sons, 2010.

[15] G. Bianchi, *IEEE P802.11 Wireless LANs, TGn Channel Models,* IEEE 802.11-03/940r4, 2004-05-10.

[16] V.J. Rhodes, *Path loss proposal for the IEEE 802.11 HTSG channel model Ad Hoc group,* April 22, 2003.

[17] J.B. Andersen, T.S. Rappaport, and S. Yoshida, "Propagation measurements and models for wireless communication channels," *IEEE Commun. Mag.,* Jan. 1995, pp. 42-49.

[18] L. Schumacher, K. I. Pedersen, and P.E. Mogensen, "From antenna spacings to theoretical capacities guidelines for simulating MIMO systems," in *Proc. PIMRC Conf.*, vol. 2, Sept. 2002, pp. 587-592.

[19] A. Perahia and R. Stacey, *Next Generation Wireless LANs - Throughput, Robustness, and Reliability in 802.11n*, Cambridge, 2008.

[20] A. Heck, *Introduction to Maple,* 3rd ed., New York: Springer-Verlag, 2003.

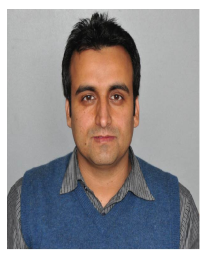

Gul Zameen Khan received a Bachelor degree in Computer Systems Engineering from University of Engineering and Technology Peshawar Pakistan in 2007 and a Master degree in Computer Engineering from Hanyang University South Korea in 2011. He is currently working as a researcher with the Intelligent Wireless Technology and Applications research group at Griffith University Australia..
He has worked as Lab Engineer in Ghulam Ishaq Khan Institute of Engineering Sciences and Technology Pakistan. In addition, he has worked as lecturer in Sarhad University of IT Peshawar Pakistan and COMSATS Institute Abbottabad Pakistan. He has also worked as a Research Assistant at Wireless Networks Lab, Dongguk University, South Korea. His areas of interest are MAC and PHY layers analysis of 802.11, multicast in Wi-Fi Direct, and wireless sensor networks.
Mr. Gul Zameen Khan is a member of IEEE and Institute for Integrated and Intelligent Systems, Griffith University Australia. He is also a professional member of Pakistan Engineering Council.

Dr. Ruben Gonzalez received a B.E. and PhD from the University of Technology, Sydney (UTS) and is currently a senior Lecturer in the School of ICT, at Griffith University Australia. He is also the director of the bachelor of computer science at Griffith University.
Previously he was founder and CTO of ActiveSky Inc, a wireless media technology company and has also held research positions at Wollongong University, OTC Ltd Research Labs and UTS. He has also held software engineering positions at various private enterprises.
Dr. Ruben Gonzalez is a member of the Institute for Integrated and Intelligent Systems, Griffith University Australia. He has over 80 refereed publications and a number of patents.

Prof. Eun-Chan Park received the B.S., M.S., and Ph.D degrees from the School of Electrical Engineering and Computer Science, Seoul National University, Seoul, Korea, in 1999, 2001, and 2006, respectively.
He worked for Samsung Electronics, Korea, as a senior engineer from 2006 to 2008. He is currently an Associate Professor in the Department of Information and Communication Engineering, Dongguk University-Seoul, Korea. He is also the head of the Wireless Networks Lab, at Dongguk University South Korea. His research interests include performance analysis, resource allocation, quality of service, congestion control, and cross-layer optimization in wired and wireless networks.
Dr. Eun-Chan Park is a member of IEEE Communications Society.

Dr. Xin-Wen Wu received the Ph.D. degree from the Chinese Academy of Sciences, Beijing, China.
He was with the Chinese Academy of Sciences; the University of California at San Diego, La Jolla, CA, USA, as a Post-Doctoral Researcher; and the University of Melbourne, Parkville, VIC, Australia, as a Research Fellow. He was with the faculty of School of Information Technology and Mathematical Science, University of Ballarat, VIC, Australia. He is currently with the faculty of School of Information and Communication Technology, Griffith University, Gold Coast, QLD, Australia.
Mr. Xin-Wen Wu is a senior member of IEEE. His research interests include cyber and data security, coding and information theory and their applications, communications and networks. He has co-authored over 70 research papers, book chapters and two books in the above-mentioned areas.